Surface Charge Distribution on DC Basin-Type Insulator

Qiandong Du, Qiaogen Zhang, Zhicheng Wu, Jingtan Ma and **Junping Zhao**
State Key Laboratory of Electric Insulation and Power Equipment,
Xi'an Jiaotong University,
710049 Xi'an, China

ABSTRACT

Surface charge accumulation on insulators is one of the bottlenecks for the development of DC electric power system. This paper studies a ±200 kV DC basin-type insulator designed for GIL (Gas-insulated Transmission Line). A surface charge measurement device is made consisting of a 3-dimension, 4-axes manipulating device, a HV shielding conductor installation system and data acquisition system. A new scaling method of the probe with an inversion algorithm using Cholesky decomposition method is proposed to obtain charge density distribution. The dynamic process of surface charge accumulation and dissipation are studied under DC voltages with different polarities, amplitudes and time durations. Charge distributions are obtained and theoretically analyzed. A novel gas-side normal electric field model is proposed for regular charge distribution and methods of suppressing surface charge are suggested, including a recommended ratio of surface and volume electric conductivity of the insulator at 1~10, structure design, and direct fluorination of the surface.

Index Terms — **DC basin-type insulator, surface charge, measurement, inverse calculation, distribution, model**

1 INTRODUCTION

GIL (Gas-insulated Transmission Line) shows promising prospects of application in electric power transmission, due to its large current carrying capacity, environmental friendliness and high reliability. Till June 2013, the total length of installed AC GIL has been more than 750 km worldwide [1,2]. Literature reports the 1 MV DC GIL of 75 m length for the ITER neutral beam injector located in Cadarache, France, but no commercial operation of long-distance DC GIL is now reported [3, 16]. The main difference between AC and DC GIL is their insulation design, including the size of coaxial electrodes, the material and structure of insulators, and the insulation properties. Notably, in the DC case, the phenomenon of charge accumulation on the surface of GIL insulators (basin-type, for example) is intractable. Charges, dust, metallic particles or other contaminants, driven by DC electric field, are prone to accumulate on insulator surface but difficult to remove. The presence of surface charge sometimes leads to the distortion of local electric field and a possible decrease of flashover voltage of insulators [2, 4]. The above problem is one of the key technological obstacles for DC GIL applications.

The eventual aim of studying surface charge phenomenon is to suppress it or control the charge density beneath an expected level. Therefore, it is essential to firstly figure out charge accumulation and dissipation dynamics. Factors that influence surface charge accumulation under DC electric field include: voltage applied, gas environment, shape and dielectric properties of insulators and surface condition of insulators [5, 6]. For the DC basin-type insulator discussed in this paper, its dielectric properties and gas environment (compressed SF_6 gas) are determined, while different voltages are related to different surface charge distributions and mechanisms, which is of great research significance.

Surface charge phenomenon has been widely studied in an international range. It is acknowledged that charge will gradually accumulate on the interface with the increase of time, which is known as the relaxation process [5, 6]. Researchers have also discovered that the polarity of charge would change with the increase of voltage amplitude [5, 26]. However, the material of insulators used for experiment is mostly AC formula epoxy resin stressed by DC voltage. But charge accumulation characteristics are different for DC formula insulator. Secondly, most studies are conducted by using epoxy resin samples or small model, few using real size basin-type insulator. Since basin-type insulator is located in GIL chamber filled with SF_6 gas, it is difficult to perform rapid and accurate charge measurement on its complex shaped surface.

The mechanism of charge accumulation on gas-solid interface has been equally studied [7]. Classic accumulation models relate to bulk, surface and gas conduction, each suitable in certain circumstances. Recent study by Tsinghua University of China shows that electron migration through bulk injection is one neglected culprit of charge accumulation and surface flashover [8]. But the true mechanism of charge transport and accumulation is still disputable. Besides, the coupled mutual

Manuscript received on 30 January 2018, in final form 16 July 2018, accepted 17 July 2018. Corresponding author: Q. Du.

DOI: 10.1109/TDEI.2018.007371

effects between surface charge and electric field is worthy of further investigation.

2 EXPERIMENT CONDITIONS

2.1 SURFACE CHARGE MEASUREMENT DEVICE

The measurement device is designed for the precise control of the probe to scan the surface of basin-type insulator. Figure 1 shows its appearance. It consists of a 3-dimensional 4-axes mechanical device inside the tank (Figure 2), a HV shielding installation system (through the tank using motive seal), and a control system. Before HVDC voltage application on the insulator, the HV shielding installation system is used to install the shielding conductor of the basin-type insulator. The shielding conductor is removed after voltage application and saved in a container inside the apparatus to leave sufficient space for probe movement.

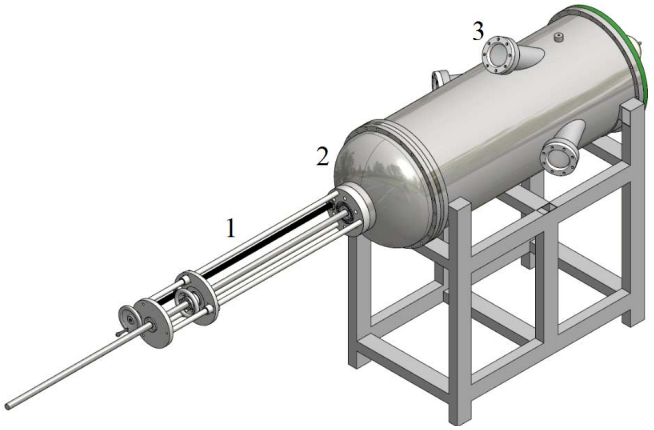

Figure 1. Appearance of surface charge measurement device (1- Rod to install or remove shielding conductor; 2-Container; 3-Observation windows).

The probe, situated at the end of the robot arm colored blue in Figure 2, is held perpendicularly to the concave surface of the insulator.

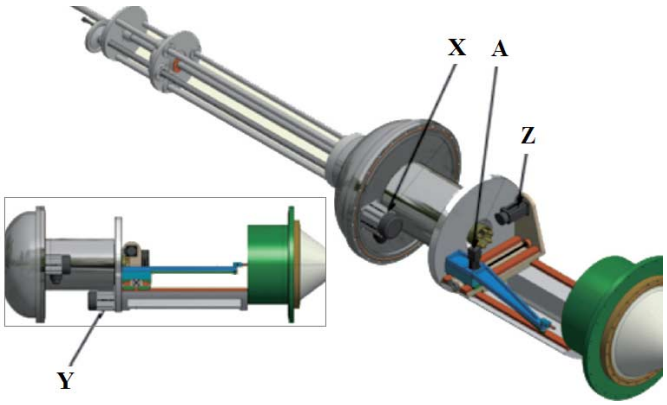

Figure 2. Profile of the 3-D 4-axes mechanical device (X, Y, Z and A are four motors that move the probe in different directions: X-rotational; Y-axial; Z-radical; A-probe angle).

PLC (Programmable Logic Controller) programs written based on the shape of insulator surface are executed for position control. The probe movement is achieved in 4 axes namely radical (Z), axial (Y), rotational (X) and gesture adjustment (A), with control precision of no more than 0.2 mm for distance, and 45' for angle. Inside the 3D 4-axes manipulating apparatus fills compressed SF_6 gas. The probe output is transferred to the outside of the device by a sealed plug and connected to the data acquisition system.

Figure 3 shows the probe scanning the surface of basin-type insulator controlled by mechanical device. Figure 4 shows the HV shielding conductor installation system which is installing/removing the shielding conductor. According to simulation analysis, the electric field induced by remained surface charges is much lower than the partial discharge inception field strength in compressed SF_6 gas. Therefore, it is ascertained that the removing of the shield dost not result in partial discharges.

Figure 3. Probe scanning the surface of insulator.

Figure 4. HV shielding conductor installation system.

The trajectory of probe on the insulator's surface can be expressed by Figure 5. The probe finishes one round and moves to another position to start the next round towards an opposite direction. At the start of each round, the mechanic system sends a signal to the data acquisition system to measure the output of the probe. At the end of each round, the mechanic system sends another signal to stop data acquisition. There are 26 rounds for the probe to scan, each with a sample frequency of 100 Hz. The entire measurement time is approximately 13 min. Follow-up experiments find that the surface charge decay time constant is several hours, therefore we assume that charge distribution remains non time varying during measurement.

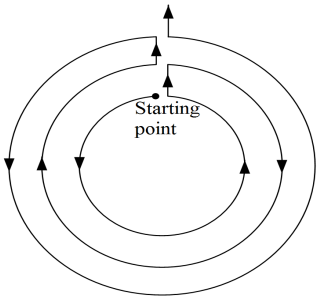

Figure 5. Movement trajectory of the probe.

2.2 EXPERIMENT SETUP AND PROCEDURE

The insulator studied in this paper is ±200 kV trial-manufactured basin-type made in DC formula, with relative permittivity being 4.9, surface electric conductivity being 8×

10^{-15} S, and volume electric conductivity being 1×10^{-14} S/m. In the experiment, the concave surface of the insulator is measured and studied. The experiment setup is shown in Figure 6. HVDC voltage is applied on the insulator through a HV bushing and GIS transfer unit. The surface charge measurement device is connected after the basin-type insulator, filled with compressed SF_6 gas of 0.3 MPa (absolute pressure). The insulator surface is cleaned by using ethyl alcohol and dried for over 6h and scanned before voltage application to ensure the non-charged state. The temperature and humidity inside the experiment tank are measured by on-line moisture monitoring system. Tests are done between 22.5 and 25.3 degree centigrade, and the moisture content in SF_6 is below 100 ppm volume fraction.

Experiment procedures are as follows: pre-treatment of DC basin-type insulator – installation of HV shielding conductor – vacuuming – inflation of SF_6 gas – (wait for over 6h) – HVDC voltage application for different time durations – immediate removal of HV shielding conductor (1min) – immediate surface charge measurement (13min).

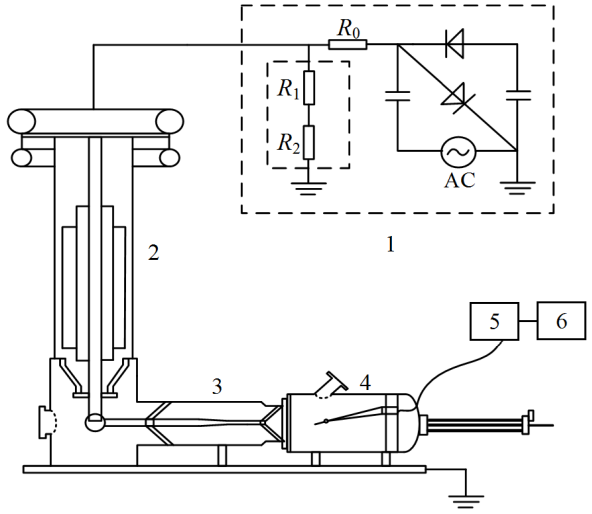

Figure 6. Experiment setup for surface charge measurement (1-HVDC generator; 2-Bushing; 3-GIS transfer unit; 4-Surface charge measurement device; 5-Charge amplifier; 6-Data acquisition system).

3 TRUSTED MEASUREMENT METHOD OF SURFACE CHARGE DENSITY

3.1 ELECTROSTATIC PROBE AND SCALING

Electrostatic probe method is used in this paper for surface charge measurement [9, 10]. The probe consists of: a central inductive probe made in red copper with a diameter of 1.5 mm, an outer shielding made in stainless steel, an insulating support made in PTFE, and a BNC connector for signal transmission to charge amplifier (Figure 7). All components are cleaned with anhydrous ethanol and dried at 25℃ for over 12 h. The charge amplifier used is Kistler 5018A. The charge induced on the probe can be directly read and exported as a 0-5 V analog signal. Its charge measurement sensitivity of 0.1 pC and quick response satisfies the request for surface charge measurement.

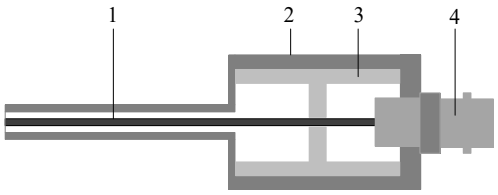

Figure 7. Structure of electrostatic probe (1-Probe; 2-Shielding; 3-PTFE support; 4-BNC connector).

The electrostatic probe works based on the principle of electrostatic induction. A new scaling method is proposed by using a set of concentric ring electrodes, in order to obtain the spatial resolution of the probe. The schematic diagram is given in Figure 8. Each ring electrode has different inner diameters but a fixed width. The set of rings covers an equivalent area as a plate electrode, while it avoids radial charge movement that happens on the latter when the probe moves. By successively applying DC voltage on each ring electrode, each response is obtained and added up for a certain distance between the fixed probe and ring center. The normalized response is then calculated. The half maximum value of the response function corresponds to the spatial resolution of the probe. At a distance d=2 mm, the probe has a spatial resolution of R_{eqv}=2.08 mm. The normalized response function is $H(r)= 1/(a+br+cr^2)$, with fitting parameters a=1.0001, b=0.9294, c= -0.0045. Here the variable r is the radius of the ring electrodes.

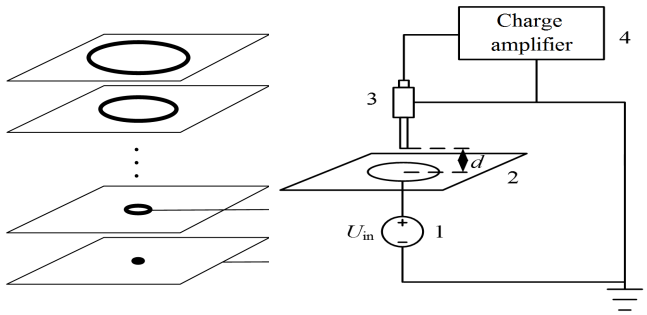

(a) A set of concentric ring electrodes (1-circuit board; 2-ring electrode).

(b) Setup for scaling the probe (1-DC voltage source; 2-ring electrode; 3-probe; 4-charge amplifier).

Figure 8. Scaling of the probe by using a set of concentric ring electrodes.

3.2 INVERSION ALGORITHM

An original matrix of dimension 26×495 can be obtained from the measurement data. Since the probe output is not merely the response of a single point but influenced by its neighbors, it is necessary to have a decoupling calculation to obtain real charge distribution.

In the radial direction, the distance between 2 neighboring points is 5 mm; in the peripheral direction, this distance scales with the diameter of the circle where it locates. After simple calculation, we find that for neighboring points, the curve distance along the insulator surface is extremely close to the straight line distance. Thus, it is unnecessary to make geometric space transformation. Considering the response function $H(x)$ defined in Chapter 3.1, 18 points are chosen

around point P (Figure 9) to calculate the real charge density at point P. The rest points are neglected since they have little influence on the response of P due to their distance.

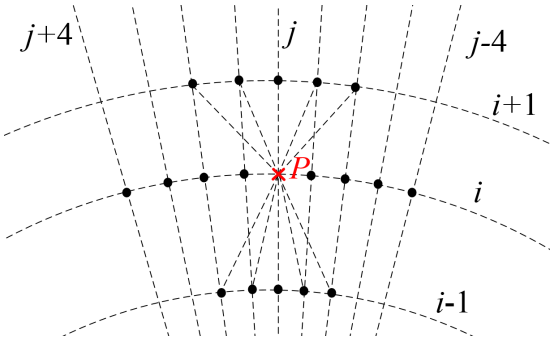

Figure 9. Choice of points for inversion calculation.

For the case in which boundaries are not taken into account, two vectors $\boldsymbol{\sigma}[1\times 19]$, $\boldsymbol{\sigma}'[1\times 19]$ and a coefficient matrix $\boldsymbol{M}[19\times 19]$ are constructed:

$$\boldsymbol{\sigma}'=\boldsymbol{M}\boldsymbol{\sigma} \quad (1)$$

where $\boldsymbol{\sigma}'$is the measured charge density of the 19 points around P (P included), $\boldsymbol{\sigma}$ is the calculated charge density of the points, in which only the element related to P is the real charge density. The elements of matrix $\boldsymbol{M}$ refers to the response coefficient $H(x)$ between two points. To solve equation (1) we must calculate the inversion of matrix $\boldsymbol{M}$, as shown in (2):

$$\boldsymbol{\sigma}=\boldsymbol{M}^{-1}\boldsymbol{\sigma}' \quad (2)$$

The Cholesky Decomposition Method is used to solve regularized linear equations (2). The principle of CDM is briefly introduced here. Since $\boldsymbol{M}$ is a positive definite matrix with its elements positive, there exists a unique invertible lower triangular matrix $\boldsymbol{G}$, so that $\boldsymbol{M} = \boldsymbol{G}\boldsymbol{G}^{\mathrm{T}}$. Thus we have $\boldsymbol{G}\boldsymbol{G}^{\mathrm{T}}\boldsymbol{\sigma}=\boldsymbol{\sigma}'$. If we suppose $\boldsymbol{G}^{\mathrm{T}}\boldsymbol{\sigma}=\boldsymbol{y}$, we have $\boldsymbol{G}\boldsymbol{y}=\boldsymbol{\sigma}'$. By solving $\boldsymbol{G}\boldsymbol{y}=\boldsymbol{\sigma}'$, $\boldsymbol{y}$ is obtained; by solving $\boldsymbol{G}^{\mathrm{T}}\boldsymbol{\sigma}=\boldsymbol{y}$, $\boldsymbol{\sigma}$ is obtained. For each loop, only one element in $\boldsymbol{\sigma}$ is the real charge density at point P.

For the case considering boundaries of the original data matrix, special treatment is conducted. For radial boundaries (i = 1 and 26), certain elements in matrix $\boldsymbol{M}$ are set to 0. For peripheral boundaries (j = 1:4 and 492:495), the 1st and 495th rows of elements are bridged. After the calculation, all points are decoupled to form a real charge density distribution figure.

4 EXPERIMENT RESULTS

4.1 CHARGE DISTRIBUTION UNDER DC VOLTGAE

4.1.1 INFLUENCE OF VOLTAGE POLARITY

The stationary distributions of basin-type insulator under DC voltages of +80 and -80 kV are shown in Figure 10. The voltage application time is 60 min. Apparently, under DC voltage of 80 kV, charge of the opposite polarity of the applied voltage accumulates on the concave surface of the insulator. Surface charge distribution is mostly circularly symmetric. The maximum charge density is more than 10 μC/m^2.

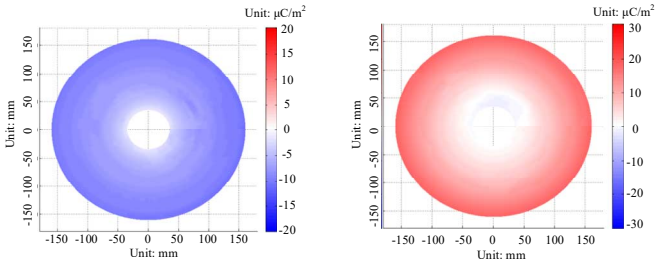

(a) U = +80 kV (b) U = -80 kV

Figure 10. Stationary surface charge distributions of DC basin-type insulator under voltages of different polarities.

The opposite charge distribution against applied voltage can be explained by the theory of charge relaxation [11]. The dynamic surface charge density $\sigma(t)$ on a gas-solid interface is expressed in Equation (3):

$$\sigma(t)=\frac{\varepsilon_s\gamma_g-\varepsilon_g\gamma_s}{b\gamma_s+a\gamma_g}U(1-e^{-t/\tau_e}) \quad (3)$$

where ε_g and γ_g are the dielectric constant and electric conductivity of gas, ε_s, γ_s are for solid. a and b are constants with length dimension, related to the structure of electrodes (or electric field distribution). U is the applied DC voltage. τ_e is the relaxation time constant. The electric field strength on the interface is defined positive from gas to solid side. For most part of the concave surface of basin-type insulator, the electric field in Equation (3) is positive. Since the voltage amplitude is rather low, the electric conductivity of gas (normally less than 10^{-18} S/m) can be neglected compared to the insulator (10^{-15} ~10^{-14} S/m). The numerator of equation (3) is negative, and surface charge has the opposite polarity to the applied voltage.

4.1.2 INFLUENCE OF VOLTAGE AMPLITUDE

The stationary distributions of basin-type insulator under different voltage amplitudes (+120, +160 and +200 kV) are shown in Figure 11. The voltage application time is 60 min.

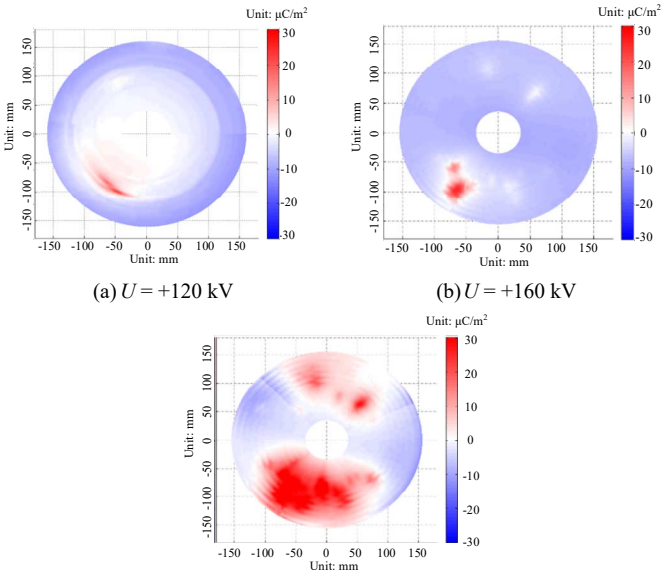

(a) U = +120 kV (b) U = +160 kV

(c) U = +200 kV

Figure 11. Stationary surface charge distributions of DC basin-type insulator under voltages of different amplitudes.

It is found that with the increase of DC voltage amplitude, some positive charge begins to accumulate at certain areas on the insulator surface. Positive charge area and its density both increase with the voltage amplitude. Voltage of high amplitudes leads to micro discharge that produces charge of the same polarity as applied voltage. Reverse of surface charge polarity happens when the voltage amplitude reaches 160 kV. Below this value, the concave surface of insulator is mostly covered by negative charge under positive DC voltage. Above this value, positive charge accumulation areas begin to expand. At U = +200 kV, the positive charge can exceed over 30 μC/m^2.

4.1.3 INFLUENCE OF VOLTAGE APPLICATION TIME

The basin-type insulator is made of DC formula material. One of the features is the electric conductivity, which is higher than AC basin-type insulator. The charging time under DC voltage stress is therefore different. Figure 12 shows surface charge distributions in the accumulation process. It is found that surface charge increases to a stationary state with the increase of voltage application time. Differing from the case of positive DC voltage application, at U = -200 kV, only negative charge accumulates on the insulator surface. The charge distribution form is determined at the early period of voltage application and does not have significant change.

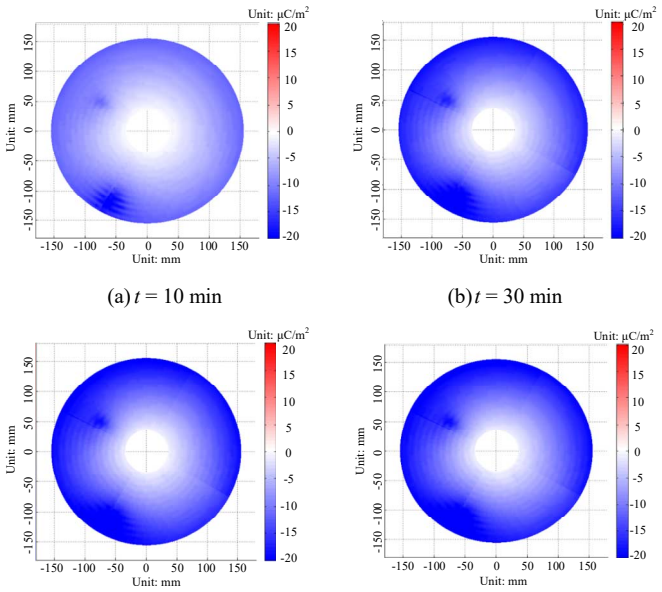

Figure 12. Surface charge distributions of DC basin-type insulator under voltages of different application times.

Figure 13 shows the average charge density varying with time. The grey region shows the range of charge densities detected on the surface. It can be seen that the charging time for DC basin-type insulator is 30~40 min. After t = 30 min, the average charge density stays at around -12 μC/m^2. The maximum value of charge density increases to the value of -35 μC/m^2. The maximum value point occurs at θ = -120° in polar coordinates, close to the outer shell of the insulator.

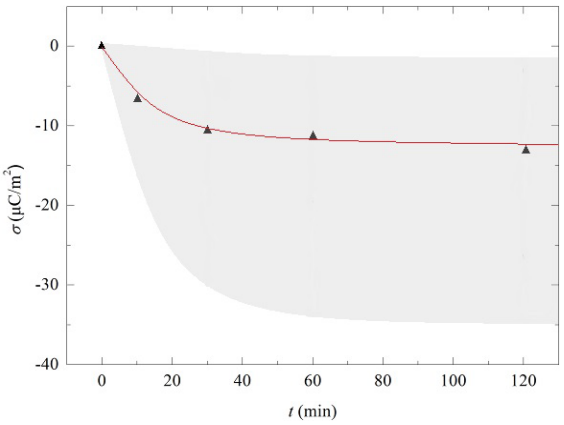

Figure 13. Surface charge density in variation of time.

The charging time constant of insulator is related to the dielectric permittivity and electric conductivity of both gas and solid materials. It is found by Kumada that the charging time constant is determined by dielectric properties of solid insulator if gas conductivity is much smaller than solid: $\tau \approx \varepsilon_s \rho_s$; else, the time constant depends on dielectric properties of gas: $\tau \approx \varepsilon_g \rho_g$. In previous studies, the insulator materials used included PMMA, PTFE and epoxy resin in AC formula, with volume resistivity higher than 10^{16} Ω·m. Therefore, in the case where gas conductivity is neglected, $\tau > \varepsilon_r \varepsilon_0 \rho_s = \varepsilon_r \times 8.85 \times 10^{-12}$ F/m$\times 10^{16}$ Ω·m$>10^5$ s=27.8 h; else, the time constant is about several tens of minutes. In this paper, the volume resistivity of DC formula insulator is much lower than that of AC formula (10^{14} Ω·m), and the charging time constant is always tens of minutes no matter the value of gas conductivity.

4.2 CHARGE DECAY CHARACTERISTICS

There are 3 ways for surface charge to dissipate: gas neutralization, surface conduction and bulk conduction. Still, surface charges remain for a long period of time on the insulator surface.

In the experiment, charge decay characteristics are studied for DC basin-type insulator. Suppose t = 0 min is the moment to cut off HVDC voltage. Figure 14 shows the charge distribution in the dissipation process. The charge distribution form does not change evidently with time. Peak values of positive and negative charge decrease, as well as the average charge density. Numerical fitting shows that the average charge density decays in exponential form (Figure 15), expressed in Equation (4):

$$\sigma(t) = \sigma_0 e^{-t/\tau_0} \tag{4}$$

Here σ_0 is the original charge density, and τ_0 the decaying time constant. τ_0 has the order of thousands of seconds. 8 h after the voltage is cut off, the charge density is below 1 μC/m^2.

$$\sigma(t) = \sigma_0 e^{-t/\tau_0} \tag{4}$$

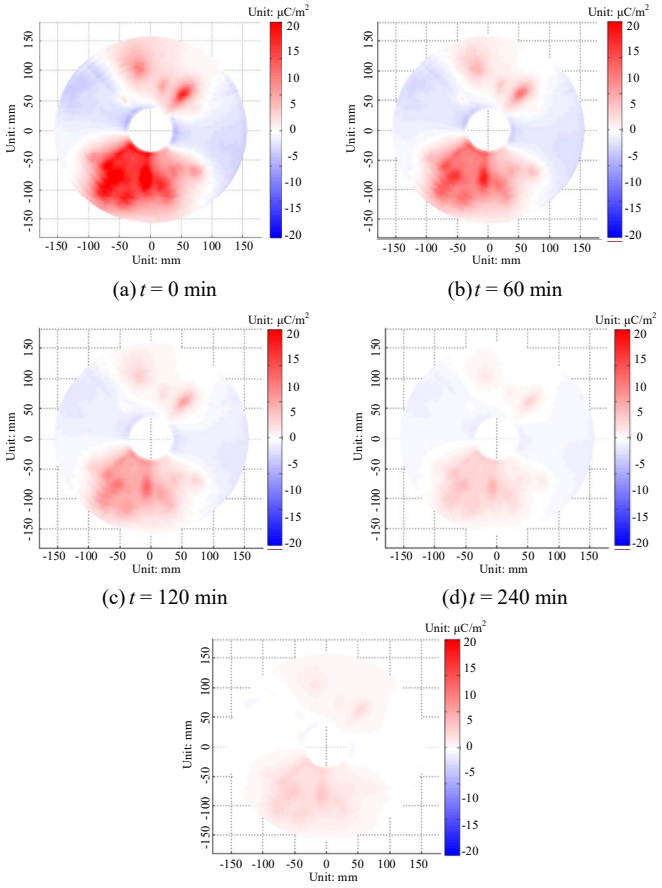

Figure 14. Surface charge distributions after cutting off HVDC voltage.

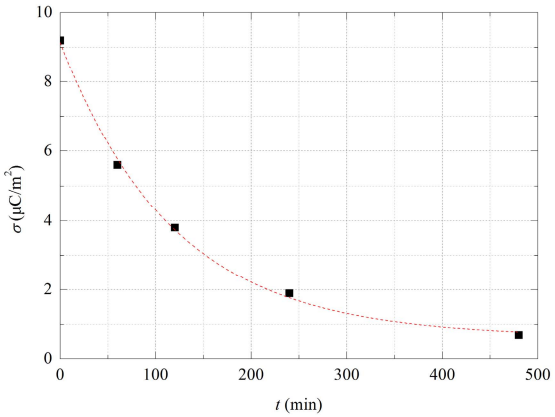

Figure 15. Decay of average charge density in variation of time.

5 DISCUSSION

5.1 INEVITIBILITY OF CHARGE ACCUMULATION

Considering the dielectric properties of both SF_6 gas and insulating material, Equation (5) is derived to describe the stationary space charge distribution in DC electric field:

$$\rho = \gamma E \cdot \nabla(\varepsilon / \gamma) \tag{5}$$

where ρ is the free charge density in the dielectric space, ε and γ are the dielectric constant and bulk electric conductivity of the dielectrics. It can be deducted from Equation (5) the inevitability of space charge accumulation inside the dielectrics. That is, for any non-isotropic dielectric material ($\nabla(\varepsilon / \gamma) \neq 0$), in the direction of leakage current, space charge accumulation occurs. Specially, on an interface where ε/γ is discontinuous, the charge accumulation phenomenon is more severe. Therefore, surface charge phenomenon is a special case of space charge accumulation. For isotropic dielectric material, the space charge density is negligible; charge mainly accumulates on the gas-solid interface.

5.2 MECHANISM OF CHARGE DISTRIBUTION

Regular charge distribution is formed in the case of low DC electric field strength. The establishment of DC electric field comes simultaneously with surface charge relaxation process, and transforms from capacitive to conductive distribution [12, 13]. Figure 16 shows the stationary DC electric field distribution at U=+80 kV. At the stationary state, the electric displacement vector $\boldsymbol{D}$ and current density $\boldsymbol{J}$ on both sides of the gas-solid interface follow Equations (6) and (7):

$$D_{ns} - D_{ng} = \sigma \tag{6}$$

$$J_{ns} = J_{ng} \tag{7}$$

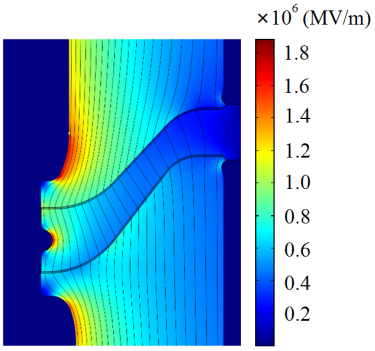

Figure 16. Stationary DC electric field distribution of the insulator at U=+80 kV.

Equations (6), (7) can be expanded in detail as (8) and (9):

$$\varepsilon_s E_{ns} - \varepsilon_g E_{ng} = \sigma \tag{8}$$

$$\gamma_s E_{ns} = \gamma_g E_{ng} \tag{9}$$

where E_{ns} and E_{ng} are the normal electric field in solid and gas side, respectively. From Equation (8) and (9), the relationship between surface charge density σ and the normal electric field in gas side E_{ng} can be derived (Equation (10)):

$$\sigma = \frac{\varepsilon_s \gamma_g - \varepsilon_g \gamma_s}{\gamma_s} E_{ng} \tag{10}$$

If the electric conductivity of SF_6 gas can be ignored compared with that of the insulator, which is the low voltage amplitude case, Equation (10) can be simplified as (11):

$$\sigma \approx -\varepsilon_g E_{ng} \tag{11}$$

To verify Equation (11), simulation is conducted in the DC electric field analysis model in *Comsol Multiphysics*. The geometric model and dielectric parameters of insulators are

entered according to the real values presented in 2.2. Mesh grid is confirmed to be precise enough and has no influence on simulation results. The electric field and surface charge distribution are obtained for the simulation model, and E_n - σ relationship is plotted in Figure 17 (red filled dots). These red filled dots are densely plotted that form the shape of a straight line. The experiment results are equally plotted (blue hollow dots), based on the measured charge density at each point under saturated condition (voltage application time is 60 min). The x-axis of Figure 17 shows the normal fields at the gaseous side under assumption of (11).

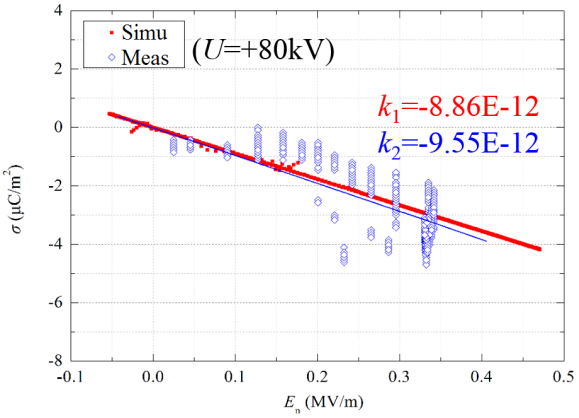

Figure 17. Relationship between normal electric field in gas side and surface charge density (Simulation and measurement).

Both simulation and measurement results are fitted using a linear function $y = ax+b$. The slope value of simulation fitted line is exactly $-\varepsilon_g = -8.86\times10^{-12}$, and that the slope value for measurement line is -9.55×10^{-12}, close to $-\varepsilon_g$. This confirms the reasonability of the normal electric field model in the explanation of regular charge distribution.

However, when the applied DC voltage has higher amplitudes and the gas conductivity is involved in the charging process, surface charge will partially begin to change polarity, and accumulate severely on the insulator. In this case, the source of surface charge includes not only the electric conduction current under DC field, but also numerous charged ions generated by gas conduction process. Experiment results in Chapter 4.1.2 show that surface charge distribution is non-uniform and random in the circumferential direction, caused by the occurrence of micro-discharge on the gas side. The reason for inception of the increased charge transport in gas include local field excess at tri-junction point, the existence of some micro defects on the insulator surface, etc.

Equation (12) describes the relationship between charge density and normal electric field at the solid side:

$$\sigma = \frac{\varepsilon_s\gamma_g - \varepsilon_g\gamma_s}{\gamma_g} E_{ns} \qquad (12)$$

If the electric conductivity of gas increases much higher than solid conductivity ($\gamma_g >> \gamma_s$) then $\sigma \approx \varepsilon_s E_{ns}$, and the normal electric field on the gas side is $E_{ng}=(\gamma_s/\gamma_g)\cdot E_{ns}\approx 0$. This shows that the existence of surface charge counteracts the normal electric field on the gas side, and surface charge accumulation reaches the stationary state. The result is equally what the gas conduction model describes.

5.3 SUPPRESSION OF SURFACE CHARGE

Methods for surface charge suppression is associated with the cause for charge accumulation, which include inner factors such as material properties, structure and surface conditions of insulator, and outer factors like applied voltage, gas type and pressure, temperature, etc. [14, 15]

For inner factors, one of the most important is the surface and volume conductivity of the DC basin-type insulator. Here α is defined as the ratio of surface and volume conductivity [unit of α: m]. α can affect the stationary field distribution by changing the resistivity of the material, and also affect the surface charge distribution by changing the leakage current. Thus α is a comprehensive criterion for dielectric optimization.

The influence of α on electric field distribution is carefully calculated by using different surface and volume conductivity values of insulator in the simulation model under +200 kV. The value of α is recommended by manufacturers is around 1 [m]. An expanded range from 10^3 to 10^{-1} [m] is chosen for the calculation. Stationary field distributions with different values of α are presented in Figure 18. Surface charge distributions are presented in Figure 19. r_{norm} is the normalized distance along the surface of insulator.

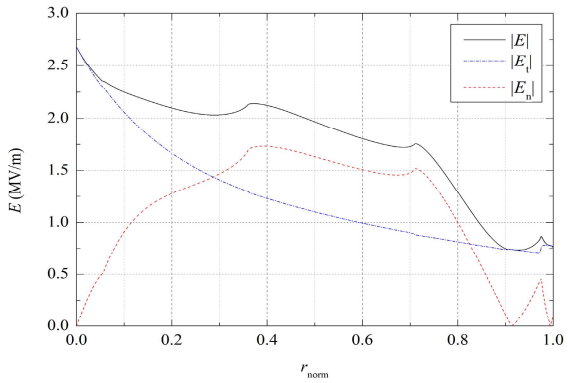

(a) $\alpha = 10^3$ [m]

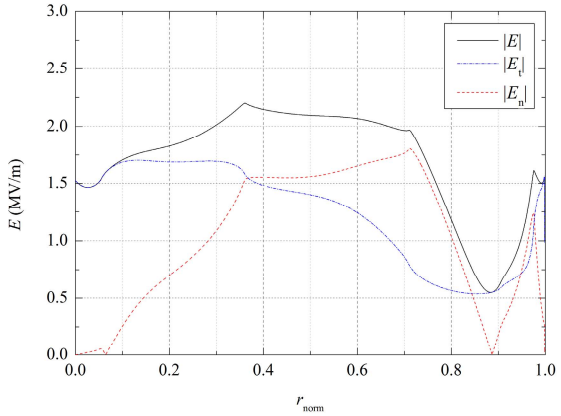

(b) $\alpha = 10^{-1}$ [m]

Figure 18. Electric field distributions with different values of α.

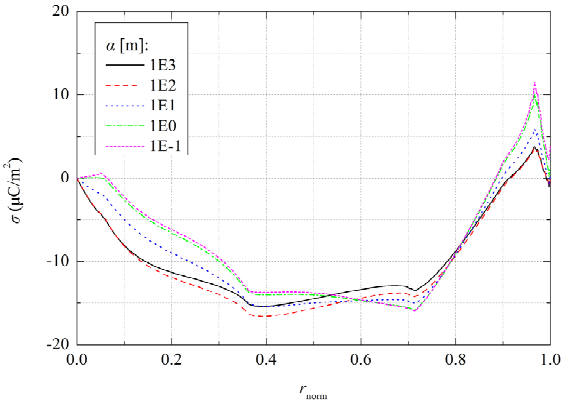

Figure 19. Surface charge distributions with different values of α.

It is found that electric field becomes more non uniform as α increases. The field non uniformity coefficient f = 1.29 when α is 10^0 [m], while f = 1.80 when α is 10^3 [m]. α is recommended to be no more than 10^1 [m] according to the field distribution analysis. When α increases from 10^{-1} to 10^2 [m], surface charge density increases due to larger surface conduction current. When α increases from 10^2 to 10^3 [m], surface charge density decreases due to a large surface conductivity and high charge decay rate. The recommended value of α is no less than 10^0 [m] to ensure charge decay rate.

Therefore, one possible method for the suppression of surface charge is the control of α in the range of 1~10 [m]. In this range, the surface electric field non uniformity is relatively low, and the charge decay time constant is calculated as several thousand seconds, in coherence with the experimental result shown in Section 4.2.

Structure design of insulator can also help to ameliorate the surface charge distribution, due to the optimized electric field distribution, which is theoretically proved by Equation (3). Structure optimization of insulator has been widely studied, with special methods used in optimization such as genetic algorithm and artificial fish swarm algorithm [16, 17].

Fluorination is proved to be an effective way to suppress surface charge. A fluorinated layer is formed to decrease the amount of the surface charges accumulated in deep traps. The surface trap density distributions and the depth of energy level decrease after the fluorination treatment [18-20]. Recent studies show that other treatments such as plasma and metal oxide coating, can also improve the surface characteristics due to the changed surface morphology and conductivity [21].

6 CONCLUSIONS

Under low voltage amplitudes, surface charge of the opposite polarity of the applied voltage accumulates on the concave surface. As the amplitude increases, charge of the same polarity as applied voltage begins to severely accumulate. The distribution is the combination of electric conduction current mechanism explained by gas-side normal electric field model, and gas conduction mechanism. For regular charge distribution, the ratio of surface charge density and normal electric field is the negative value of gas electric permittivity.

Methods of surface charge suppression are proposed, such as the control of α value in the range of 1~10 [m], structure optimization of basin-type insulator, and fluorination or other surface treatment.

ACKNOWLEDGEMENT

This study is financially supported by Science and Technology Project of State Grid Corporation of China (SGSXCZ00XTJS1700081).

REFERENCES

[1] H. Koch. *Gas-insulated transmission lines (GIL)*. Hoboken: Wiley-IEEE Press, 2012, pp.21-25.

[2] P. Li. "Flashover characteristics along the insulator in SF_6 Gas under DC voltage and its application in UHV DC GIL," PhD dissertation, Xi'an Jiaotong Univ., China, 2015.

[3] R. Aymar, P. Barabaschi and Y. Shimomura. "The ITER design,". Plas. Phys. Contr. Fus. vol. 44(5), 519, 2002.

[4] F. Wang. "Research on surface charge accumulation and its effect on flashover characteristics of the insulator," PhD dissertation, Xi'an Jiaotong Univ., China, 2003.

[5] J. Tan. "Surface charge accumulation in SF_6," PhD dissertation, Delft Univ. of Tech., Netherlands, 1993.

[6] H. Fujinami, T. Takuma, M. Yashima and T. Kawamoto. "Mechanism and effect of DC charge accumulation on SF_6 gas insulated spacers," IEEE Trans. Pow. Del., vol. 4(3), pp. 1765-1772, 1989.

[7] G. Ma, H. Zhou, C. Li, J. Jiang and X. Chen. "Designing epoxy insulators in SF_6-filled DC-GIL with simulations of ionic conduction and surface charging," IEEE Trans. Dielectr. Electr. Insul., vol. 22(6), pp. 3312-3320, 2016.

[8] C. Li, J. Hu, C. Lin and J. He. "The potentially neglected culprit of DC surface flashover: electron migration under temperature gradients," Scientific Reports, vol. 7(1), 3271, 2017.

[9] H. Ootera and K. Nakanishi. "Analytical method for evaluating surface charge distribution on a dielectric from capacitive probe measurement - application to a cone-type spacer in + or - 500 kV DC-GIS," IEEE Trans. Pow. Del., vol. 3(1), pp. 165-172, 2002.

[10] D. Faircloth and N. Allen. "High resolution measurements of surface charge densities on insulator surfaces," IEEE Trans. Dielectr. Electr. Insul., vol. 10(2), pp. 285-290, 2003.

[11] C. Feng and X. Ma. *Introduction to engineering electromagnetic fields*. Beijing: H. Edu. Pr., 2000, pp. 74-79.

[12] A. Winter and J. Kindersberger. "Stationary resistive field distribution along epoxy resin insulators in air under DC voltage," IEEE Trans. Dielectr. Electr. Insul., vol. 19(5), pp. 1732-1739, 2012.

[13] A. Winter and J. Kindersberger. "Transient field distribution in gas-solid insulation systems under DC voltages," IEEE Trans. Dielectr. Electr. Insul., vol. 21(1), pp. 116-128, 2014.

[14] J. Kindersberger and C. Lederle. "Surface charge decay on insulators in air and sulfurhexafluorid – Part I: Simulation," IEEE Trans. Dielectr. Electr. Insul., vol. 15(4), pp. 941-948, 2008.

[15] J. Kindersberger and C. Lederle. "Surface charge decay on insulators in air and sulfurhexafluorid – Part II: Measurements," IEEE Trans. Dielectr. Electr. Insul., vol. 15(4), pp. 949-957, 2008.

[16] A. De Lorenzi, L. Grando, A. Pesce, P. Bettini and R. Specogna. "Modeling of epoxy resin spacers for the 1 MV DC gas insulated line of ITER neutral beam injector system," IEEE Trans. Dielectr. Electr. Insul., vol. 16(1), pp. 77-86, 2009.

[17] E. Volpov. "Dielectric strength coordination and generalized spacer design rules for HVAC/DC SF_6 gas insulated systems," IEEE Trans. Dielectr. Electr. Insul., vol. 11(6), pp. 949-963, 2004.

[18] B. Zhang, Z. Qi and G. Zhang. "Charge accumulation patterns on spacer surface in HVDC gas-insulated system: Dominant uniform charging and random charge speckles," IEEE Trans. Dielectr. Electr. Insul., vol. 24(2), pp. 1229-1238, 2017.

[19] B. Zhang, G. Zhang, Q. Wang, C. Li, J. He and Z. An. "Suppression of surface charge accumulation on Al_2O_3-filled epoxy resin insulator under DC voltage by direct fluorination," AIP Advances, vol. 5(12), pp. 1-12, 2015.

[20] C. Li, J. He, J. Hu, "Surface morphology and electrical characteristics of direct fluorinated epoxy-resin/alumina composite," IEEE Trans. Dielectr. Electr. Insul., vol. 23(5), pp. 3071-3077, 2016.
[21] C. Li, J. Hu, C. Lin and J. He. "The control mechanism of surface traps on surface charge behavior in alumina-filled epoxy composites", J. Phys. D: Appl. Phys., vol. 49(44), 445304, 2016.